



## Migration and distribution of saline ions in bauxite residue during water leaching

Xiang-feng KONG<sup>1,2</sup>, Xing-xing JIANG<sup>1,2</sup>, Sheng-guo XUE<sup>1,2</sup>,  
Ling HUANG<sup>1,2</sup>, William HARTLEY<sup>3</sup>, Chuan WU<sup>1,2</sup>, Xiao-fei LI<sup>1,2</sup>

1. School of Metallurgy and Environment, Central South University, Changsha 410083, China;
2. Chinese National Engineering Research Center for Control & Treatment of Heavy Metal Pollution, Central South University, Changsha 410083, China;
3. Crop and Environment Sciences Department, Harper Adams University, Newport, Shropshire, TF10 8NB, United Kingdom

Received 3 January 2017; accepted 24 April 2017

**Abstract:** Bauxite residue, a highly saline solid waste produced from digestion of bauxite for alumina production, is hazardous to the environment and restricts vegetation establishment in bauxite residue disposal areas. A novel water leaching process proposed here was used to investigate the dynamic migration and vertical distribution of saline ions in bauxite residue. The results show that water leaching significantly reduced the salinity of bauxite residue, leaching both saline cations  $\text{Na}^+$ ,  $\text{K}^+$ ,  $\text{Ca}^{2+}$  and anions  $\text{CO}_3^{2-}$ ,  $\text{SO}_4^{2-}$ ,  $\text{HCO}_3^-$ .  $\text{Na}^+$  and  $\text{K}^+$  migrated from 40–50 to 20–30 cm of the column, presenting a high migration capacity. The migration capacity of  $\text{Ca}^{2+}$  was lower and accumulated at 30–40 cm of the column.  $\text{CO}_3^{2-}$  initially distributed at 20–30 cm of the column, subsequently transported to 30–40 cm of the column, and finally returned to 20–30 cm of the column along with evaporation.  $\text{SO}_4^{2-}$  was originally distributed at 40–50 cm, but finally migrated to 20–30 cm of the column. Nevertheless,  $\text{HCO}_3^-$  remained at the bottom of the column, and its migratory was less affected by evaporation.

**Key words:** bauxite residue; salinity; ion migration; column stimulation; water leaching

### 1 Introduction

The alumina industry has developed rapidly due to the requirement for aluminum. Unfortunately, such rapid development has brought about multiple environmental problems that profoundly influence the sustainable development [1–3]. Bauxite residue (BR, or red mud) is a highly saline solid byproduct generated during alumina extraction from bauxite using Bayer, sintering and combined Bayer-sintering processes in alumina refineries. The volume of BR generated while producing 1 t of alumina is typically 0.5–2 t [4–7]. The cumulative global inventory of BR has reached an estimated 4 billion tons, and is still increasing [8–10]. Many efforts have been made to find suitable uses for BR, but as yet no economic method has been extensively applied [11–13]. Therefore, almost all BR continues to

be disposed in BRDAs [14,15], which requires sustainable efforts to manage the waste [16,17]. Furthermore, freshly formed saline dusts on the surface of BRDA containing large concentrations of salts are harmful to the surrounding environment [18–20]. The elevated salts mean that BR is a hazardous waste, which limit its safe disposal and revegetation.

High salinity is a result of using sodium hydroxide for extracting alumina from the ore and the formation of a complex-saline mineral. The residual sodium carbonate ( $\text{Na}_2\text{CO}_3$ ) and sodium bicarbonate ( $\text{NaHCO}_3$ ) that can not be completely separated by counter-current decantation (CCD) water washing before disposal partly remain in BR, and are responsible for the soluble-sodic salinity [21,22]. Additionally, potash ( $\text{K}_2\text{CO}_3$ ) and  $\text{Na}_2\text{SO}_4$  commonly exist in BR. Furthermore, The formed solid phase of tri-calcium aluminate (TCA,  $\text{Ca}_3\text{Al}_2(\text{OH})_{12}$ ), cancrinite ( $\text{Na}_6\text{Al}_6\text{Si}_6\text{O}_{24}\cdot 2\text{CaCO}_3$ ),

sodalite ( $\text{Na}_6\text{Al}_6\text{Si}_6\text{O}_{24}\cdot\text{Na}_2\text{CO}_3$ ), and hydrogarnet ( $\text{Ca}_3\text{Al}_2(\text{SiO}_4)_x(\text{OH})_{12-4x}$ ) are typical buffering minerals [23,24], which act as another source of salinity.

The removal of BR salinity is therefore critical. Nevertheless, many efforts are to remove or transform the alkalinity of BR, which are commonly applied by alumina refinery to treat with BR prior to store and ameliorate for revegetation at BRDAs [25,26]. The addition of gypsum, organic matter and fertilizer, seawater neutralization, waste acid interaction and carbon dioxide sequestration have been attempted to reduce and/or remove the high alkalinity [27,28]. Nevertheless, removal and separation of salinity have only been minimal. Water washing is a promising way forward in an attempt to reduce the strong alkalinity and remove the high salinity; this may leach approximately 70% alkaline Na whilst also reducing a large proportion of salts [29]. However, information on migration behavior of saline compounds and their subsequent distribution is absent, but is significant if a well-founded transportation-migration theory is to be understood. Furthermore, less concern has been paid to saline migration in BRDAs. Indeed, lack of understanding of dynamic migration and vertical distribution of saline ions in BR during water leaching is a knowledge gap that requires attention.

The objectives of the present study are to investigate leaching and migration behaviors of saline cations and anions in bauxite residue using a column leaching study, and to research the vertical distribution of saline ions in residue during long-term leaching.

## 2 Experimental

### 2.1 Field sampling and sample preparation

In October 2015, a raw BR sample, used throughout this study, was collected from an Aluminum Refinery Corporation of China. The freshly stored BR was collected from the surface of BRDA's. Three sub-samples were collected with a distance of 10 m from each other to obtain a uniform sample (Fig. 1(a)). Samples were stored in polyethylene bags, returned to the laboratory and subsequently air-dried for 4 d, and then sieved to retain the <2 mm fraction. SEM image of the sample (Fig. 1(b)) showed that it consisted of 0.1–0.5  $\mu\text{m}$  particles in 2–10  $\mu\text{m}$  aggregates, which was poorly-crystallized. Compositions of BR are presented in Table 1.

### 2.2 Long-term leaching experiment

The leaching experiment was conducted using a column (Fig. 2) to simulate long-term leaching by rainfall in a BRDA. Two half-cylinders were bonded to create the column with an outer diameter of 14 cm, an inner diameter of 12.6 cm and a height of 95 cm, and 36 sample holes were pre-drilled and arranged on the outer wall for convenient sampling at various time during the investigation. The column base was mesh, being supported with a 5 cm depth of sand. Subsequently, the column was filled with BR, and Milli-Q water was supplied slowly from the bottom of the column. After 2 d of saturation, Milli-Q water was then supplied slowly

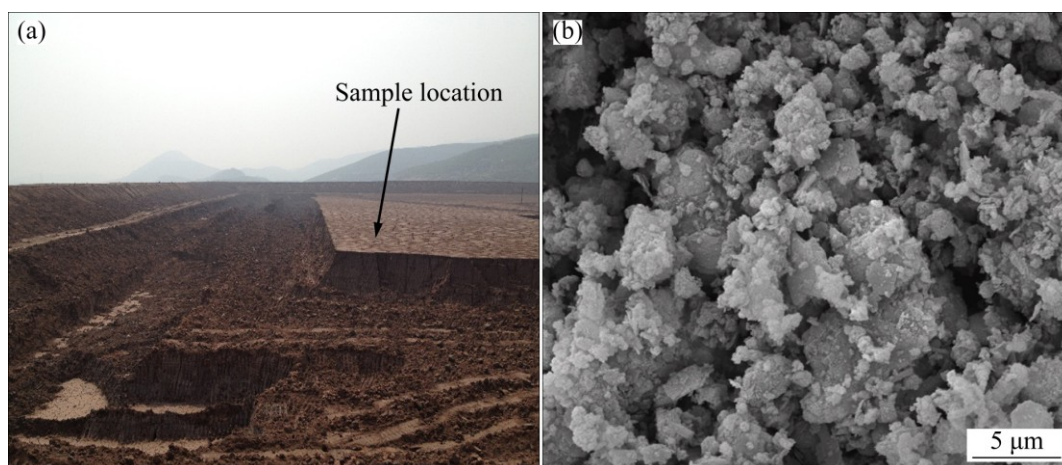


**Fig. 1** Bauxite residue sample collected from surface of BRDA (a) and SEM image of bauxite residue (b)

**Table 1** Initially saline composition of bauxite residue in water leaching column experiment

Concentration of saline cations/( $\text{mmol}\cdot\text{kg}^{-1}$ )				Concentration of saline anions/ ( $\text{mmol}\cdot\text{kg}^{-1}$ )			Electric conductivity/ ( $\text{mS}\cdot\text{cm}^{-1}$ )	pH
$\text{Na}^+$	$\text{K}^+$	$\text{Ca}^{2+}$	$\text{Mg}^{2+}$	$\text{CO}_3^{2-}$	$\text{HCO}_3^-$	$\text{SO}_4^{2-}$		
132.16	10.72	0.30	–	57.00	6.53	7.51	1.80	11.05

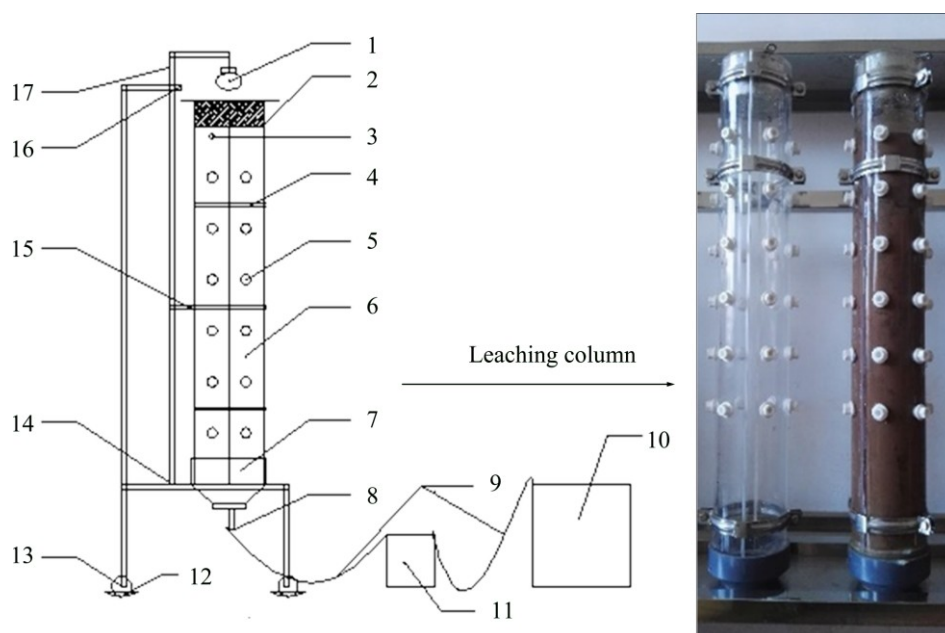


**Fig. 2** Leaching column of bauxite residue for simulating long-term leaching of BRDA (1—Infrared lamp; 2—Water distributor; 3—First inlet; 4—Fixed clip (top); 5—Sampling valve; 6—Cylinder; 7—Substructure; 8—Second inlet or outlet; 9—Hose; 10—Water collector; 11—Peristaltic pump; 12—Brake block; 13—Pulley; 14—First pedestal; 15—Fixed clip (middle); 16—Second pedestal; 17—Motion bar)

from the top, controlling the water level 5 cm above the surface of the packed residue. Leachate was immediately collected from the bottom until no further liquor was produced, whilst the mass of each leachate was measured. After leaching, the leached residues were collected at depths of 15, 25, 35, 45, 55 and 65 cm at regular intervals.

### 2.3 Sample analysis

The leachate was centrifuged at 4000 r/min for 10 min and then analyzed for pH with a probe calibrated to a slope >99%, meanwhile determining electric conductivity (EC) with a probe calibrated to electrode constant  $K=1.00 (\pm 0.05)$  in a 2.76 mS/cm solution. Soluble  $\text{Na}^+$ ,  $\text{K}^+$  and  $\text{Ca}^{2+}$  concentrations in leachate were analyzed by a PerkinElmer Optima 5300 ICP–AES. Saline  $\text{CO}_3^{2-}$  and  $\text{HCO}_3^-$  were analyzed by titration using 0.02 mol/L  $\text{H}_2\text{SO}_4$  standardized solution [24], and  $\text{SO}_4^{2-}$  was determined on a Daian ICS-90A HPIC. Residual solids collected from the column were oven-dried at 65 °C and sieved to retain the <0.38  $\mu\text{m}$  fraction. Subsequently, soluble ions were extracted by water from the residues and analyzed.

## 3 Results and discussion

### 3.1 Change of saline cation concentration in leachate

The changes of  $\text{Na}^+$ ,  $\text{K}^+$  and  $\text{Ca}^{2+}$  concentrations in leachate presented in Fig. 3 show that they changed

slightly in 76 min of leaching. However, after 76 min, soluble  $\text{Na}^+$  increased with leaching time, but soluble  $\text{Ca}^{2+}$  decreased sharply, whilst soluble  $\text{K}^+$  remained stable. Soluble  $\text{Na}^+$  concentration increased from 14.13 mmol/L at 76 min to 43.74 mmol/L at 467 min, subsequently, reaching equilibrium. Soluble  $\text{Ca}^{2+}$  concentration decreased from 1.90 mmol/L at 76 min to 0.38 mmol/L at 400 min.

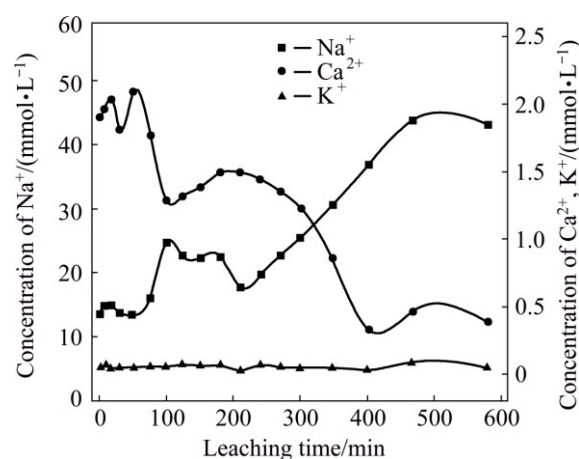


**Fig. 3** Concentrations of saline cations  $\text{Na}^+$ ,  $\text{K}^+$  and  $\text{Ca}^{2+}$  in leachate

Soluble saline cation results (Fig. 3) indicated that the changes in their concentrations were relatively consistent at 76 min of leaching. During 76 min leaching, the leachate did not penetrate and just moved to the

bottom of the column. The leachate collected from the column was a saturated solution of BR and the saline  $\text{Na}^+$ ,  $\text{K}^+$  and  $\text{Ca}^{2+}$  only dissolved in pore water of BR, which did not start to migrate. After 76 min leaching, the concentration of soluble  $\text{Na}^+$  increased in leachate, showing that a large amount of  $\text{Na}^+$  was leached, further confirming that soluble  $\text{Na}^+$  dominated the soluble cations in the leachate. Furthermore, soluble  $\text{Na}^+$  indicated that the colloidal adsorption of  $\text{Na}^+$  was weak, being affected by ion concentration, ionic radius and charge, further suggesting that its leaching capacity with water was strong and the leaching process may promote its removal. However, soluble  $\text{Ca}^{2+}$  in leachate decreased, and colloidal adsorption would profoundly influence its mobility due to its ionic charge and larger ionic radius. This suggested that the  $\text{Ca}^{2+}$  migration capacity with water was limited and did not improve its removal. The leaching of  $\text{K}^+$ , however, was relatively stable. Therefore, it may be summarized that the leaching capacity of various saline cations in BR were in the following decreasing order:  $\text{Na}^+ > \text{K}^+ > \text{Ca}^{2+}$ .

### 3.2 Change of saline anion concentration in leachate

The concentration changes of  $\text{CO}_3^{2-}$ ,  $\text{HCO}_3^-$  and  $\text{SO}_4^{2-}$  in leachate are presented in Fig. 4, which revealed that they increased during the leaching process. Nevertheless, the concentration of  $\text{CO}_3^{2-}$  was approximately 1.0 mmol/L within 240 min, subsequently increasing to 7.16 mmol/L at 400 min. The concentration of  $\text{SO}_4^{2-}$  increased from 5.10 mmol/L at 100 min to 8.01 mmol/L at 400 min, whilst  $\text{HCO}_3^-$  in leachate increased rapidly after 76 min, reaching approximately 14.0 mmol/L at 500 min.

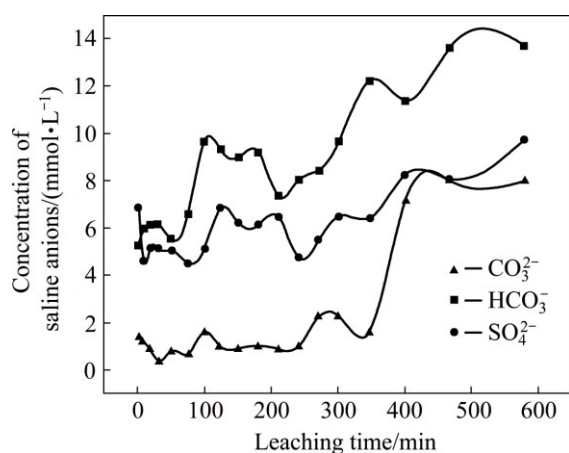


Fig. 4 Concentrations of saline anions  $\text{CO}_3^{2-}$ ,  $\text{HCO}_3^-$  and  $\text{SO}_4^{2-}$  in leachate

Soluble saline anion results (Fig. 4) indicated that the changes in the concentrations of  $\text{CO}_3^{2-}$ ,  $\text{HCO}_3^-$  and  $\text{SO}_4^{2-}$  in leachate were uniform within 76 min. The leachate also did not penetrate and just moved to the

bottom of the column and the saline  $\text{CO}_3^{2-}$ ,  $\text{HCO}_3^-$  and  $\text{SO}_4^{2-}$  only existed in the saturated solution from the BR. After 76 min leaching,  $\text{HCO}_3^-$  concentration in leachate clearly increased, and a large of  $\text{HCO}_3^-$  was leached. Additionally, the concentration of  $\text{HCO}_3^-$  was greater than that in the original BR (Table 1), indicating colloid adsorption of  $\text{HCO}_3^-$  was weak, suggesting that the leaching capacity of  $\text{HCO}_3^-$  with water was strong, promoting  $\text{HCO}_3^-$  removal. A similar change for  $\text{SO}_4^{2-}$  concentration was observed, but the change was delayed by approximately 30 min. However, the concentration of  $\text{CO}_3^{2-}$  later increased, which was even lower than that in initial BR (Table 1). Less  $\text{CO}_3^{2-}$  was leached into the leachate, which was deeply affected by colloid adsorption as a result of its multiple ionic charge similar to  $\text{Ca}^{2+}$ . Thus, the leaching capacities of saline anions in BR were in the following decreasing order:  $\text{HCO}_3^- > \text{SO}_4^{2-} > \text{CO}_3^{2-}$ .

### 3.3 Vertical distribution of saline cations in residue

The vertical distributions of  $\text{Na}^+$ ,  $\text{K}^+$  and  $\text{Ca}^{2+}$  in the residue of the leaching column at different time are shown in Fig. 5. The  $\text{Na}^+$  distribution at 0–60 cm (Fig. 5(a)) shows that the peaks of  $\text{Na}^+$  concentrations in the vertical distribution were located at 45.33 cm at 2 d following the leaching episode, 34.69 cm at 14 d following the leaching episode, and 28.89 cm at 26 d following the leaching episode, respectively. At the beginning of stage following the leaching episode, the liquors continuously penetrated downward under the function of capillary pressure and gravity, meanwhile the intermolecular force interaction between  $\text{Na}^+$  and hydrone was stronger than the force between  $\text{Na}^+$  and the colloidal particle of BR, which resulted in the high migration of  $\text{Na}^+$  at a column depth of 40–50 cm. In later period of leaching, capillary pressure disappeared whilst the leached liquors were affected by evaporation, which changed the distribution of liquor and further promoted the upward migration of  $\text{Na}^+$ , resulting in a concentration peak of  $\text{Na}^+$  re-distribution located at 20–30 cm.

The distribution of  $\text{Ca}^{2+}$  in the column at depths of 0–60 cm (Fig. 5(b)) revealed that the peaks of  $\text{Ca}^{2+}$  concentration were situated at 33.17 cm after 2 d of leaching, 25.84 cm, after 14 d of leaching, and 26.66 cm after 26 d of leaching, respectively. At the initial stage following the leaching episode, the intermolecular force interaction between  $\text{Ca}^{2+}$  and hydrone was higher than the force between  $\text{Ca}^{2+}$  and the colloidal particles of BR. However,  $\text{Ca}^{2+}$  was distributed at 30–40 cm of the column, which demonstrated a relatively weak migration compared to the  $\text{Na}^+$  distribution at the depths of 40–50 cm. This may be due to the multiple ionic charge and large ionic radius (Fig. 2). Later, with a reduction in liquor infiltration and intermolecular force interaction

between  $\text{Ca}^{2+}$  and hydronium, the migration of  $\text{Ca}^{2+}$  became more difficult, resulting in the peak of  $\text{Ca}^{2+}$  fixed at approximately 26 cm. Besides, the peak value of  $\text{Ca}^{2+}$  concentration was 0.26 mmol/kg in the initial stage following leaching; however, it decreased to

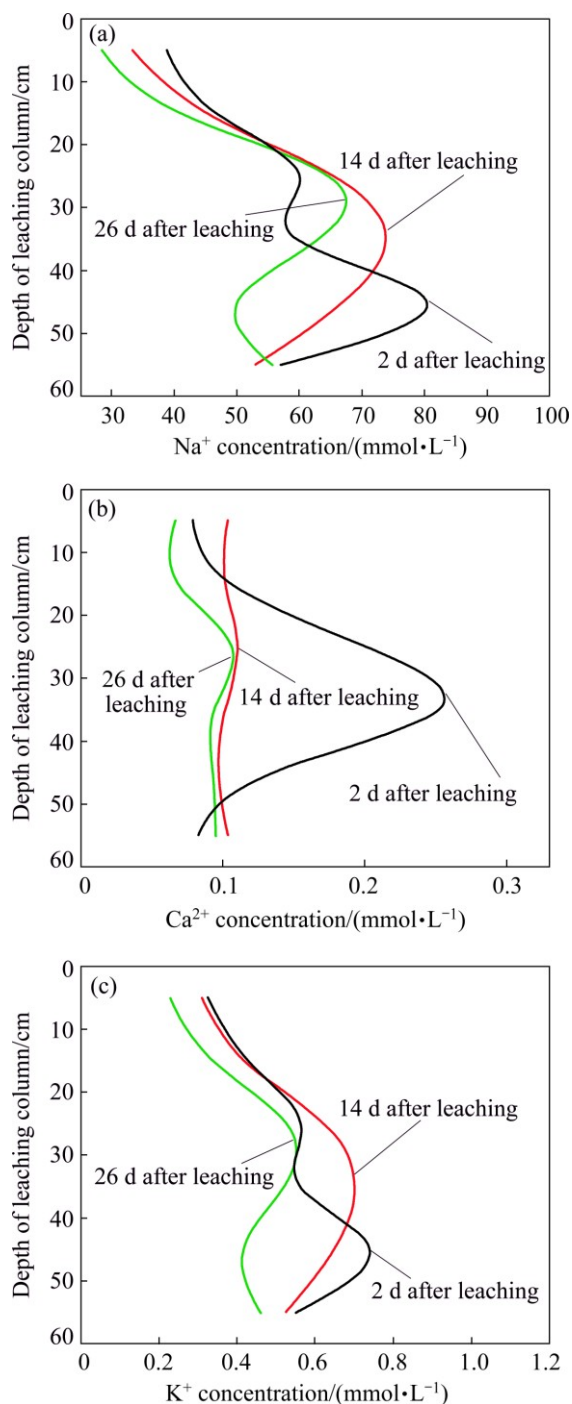


**Fig. 5** Vertical distribution of saline cations  $\text{Na}^+$  (a),  $\text{Ca}^{2+}$  (b) and  $\text{K}^+$  (c) in residue after leaching (The distributions of  $\text{Na}^+$ ,  $\text{K}^+$  and  $\text{Ca}^{2+}$  concentrations at 8, 20, and 32 d following the leaching episode, have been concealed to enhance the visibility of the peaks. The peaks of 8 and 20 d were located in the interaction between 2 and 14 d, and between 14 and 26 d, respectively. Additionally, the distribution of 32 d was similar to that of 26 d)

approximately 0.10 mmol/L which was reduced by 60%. Meanwhile, the peak value of  $\text{Na}^+$  concentration was slightly reduced compared to  $\text{Ca}^{2+}$ . This distribution characteristic suggested that  $\text{Na}^+$  was replaced with  $\text{Ca}^{2+}$  in the initial period following leaching.

The  $\text{K}^+$  distribution at depths of 0–60 cm (Fig. 5(c)) proves that the peaks of  $\text{K}^+$  concentration were located at 45.46 cm and 2 d following the leaching episode, 35.24 cm at 14 d following the leaching episode, and 29.00 cm at 26 d following the leaching episode, respectively. The  $\text{K}^+$  distribution characteristic was similar to that of  $\text{Na}^+$ . At the front-end after leaching,  $\text{K}^+$  had a high migration rate and concentrated at 40–50 cm of the column. In the later period after leaching, evaporation changed the distribution of liquor and improved the upward migration of  $\text{K}^+$ , which resulted in a concentration peak of  $\text{K}^+$  re-distributed to 20–30 cm.

### 3.4 Vertical distribution of saline anion in residue

The distribution characteristics of saline anions in the residue depict a discrepant change with that of saline cations, as presented in Fig. 6. The  $\text{CO}_3^{2-}$  distribution of the residue in the leaching column at depths of 0–60 cm (Fig. 6(a)) shows that the peaks of  $\text{CO}_3^{2-}$  concentrations in the vertical distribution were located at 24.33 cm at 2 d after leaching, 33.58 cm at 14 d after leaching, and 26.12 cm at 26 d after leaching, respectively. In the initial period of leaching,  $\text{CO}_3^{2-}$  ions at the top of the column penetrated downward along with the liquor. Nevertheless, the migration capacity of  $\text{CO}_3^{2-}$  is weak due to its multiple ionic charge and larger ionic radius, which resulted in the reduced migration rate of  $\text{CO}_3^{2-}$  at depths of 20–30 cm. At 14 d following the leaching episode, the peak of  $\text{CO}_3^{2-}$  gradually migrated to depths of 30–40 cm. However, in the final period of leaching, the infiltrated pressure was reduced, whilst the leached liquors were influenced by evaporation, which returned to depths of 20–30 cm.

The  $\text{HCO}_3^-$  distribution of the residue in the leaching column at depths of 0–60 cm (Fig. 6(b)) shows that the peaks of  $\text{HCO}_3^-$  concentration in the vertical distribution were located at 32.76 cm after leaching for 2 d, 55.55 cm after leaching for 14 d, and 42.98 cm after leaching for 26 d following the leaching episode, respectively. At the beginning of stage following the leaching episode, the peak of  $\text{HCO}_3^-$  concentration moved from depths of 32.76 to 55.55 cm, which manifested a high capacity of migration which is in agreement with its leaching capacity. In the medium period, with the capillary pressure and penetrated pressure becoming weak, the migration slowed down. Subsequently, the effect of evaporation was higher than that of the pressure, which resulted in the  $\text{HCO}_3^-$  migrating upwards. However, the peak of  $\text{HCO}_3^-$

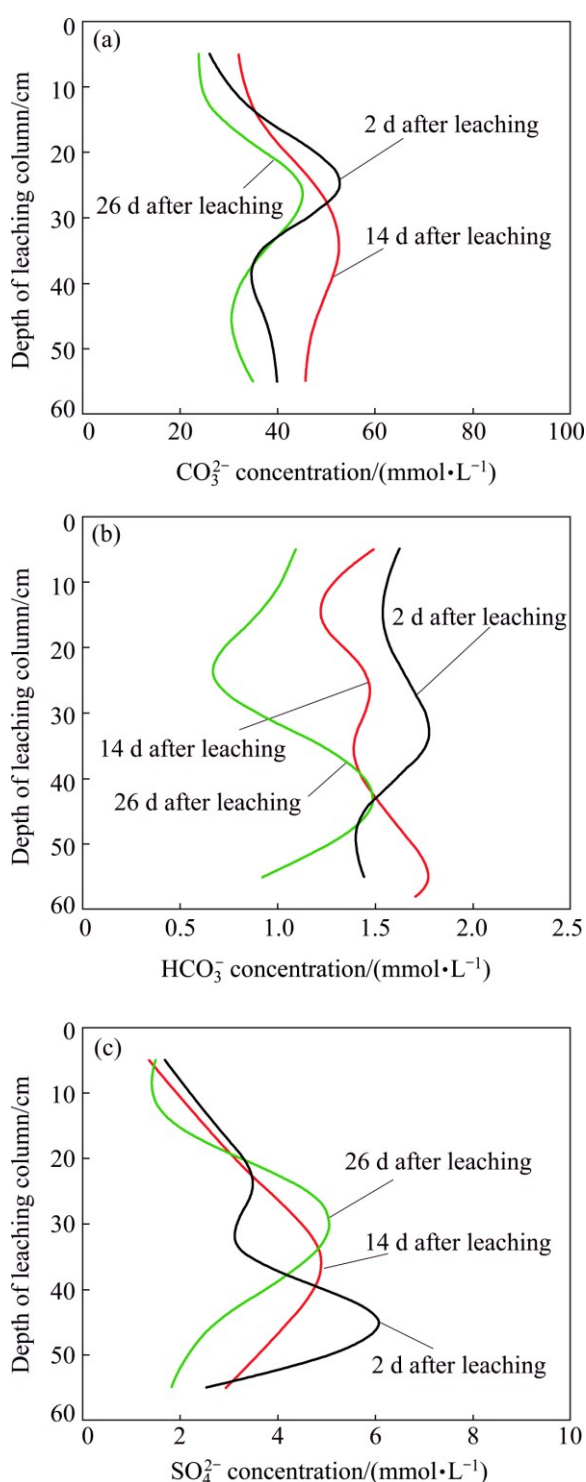


**Fig. 6** Vertical distribution of saline anions  $\text{CO}_3^{2-}$  (a),  $\text{HCO}_3^-$  (b) and  $\text{SO}_4^{2-}$  (c) in residue after leaching at different time (Distribution of  $\text{CO}_3^{2-}$ ,  $\text{HCO}_3^-$  and  $\text{SO}_4^{2-}$  concentrations at 8, 20 and 32 d following the leaching episode has been omitted to enhance the visibility of the peaks. Peaks of  $\text{CO}_3^{2-}$ ,  $\text{HCO}_3^-$  and  $\text{SO}_4^{2-}$  concentrations at 8 and 20 d were located in the interaction between 2 and 14 d, and between 14 and 26 d, respectively. Additionally, distribution of  $\text{CO}_3^{2-}$ ,  $\text{HCO}_3^-$  and  $\text{SO}_4^{2-}$  concentrations at 32 d was similar to that of 26 d besides  $\text{HCO}_3^-$  with the peak lower than that at 26 d)

concentration was fixed at 40–50 cm instead of higher depths of 30–40 cm or 20–30 cm, although the  $\text{HCO}_3^-$  has a strong capacity of migration. Bicarbonate ions showed a reverse change, suggesting that the migration of  $\text{HCO}_3^-$  was less affected by evaporation. At the final stage, the major  $\text{HCO}_3^-$  remained at the bottom of the leaching column rather than on the surface. The migration characteristics of  $\text{HCO}_3^-$  may avoid the occurrence of its efflorescence, further implying that leaching is helpful to control the salinity of BR.

The  $\text{SO}_4^{2-}$  distribution of the residue at depths of 0–60 cm (Fig. 6(c)) shows that the peaks of  $\text{SO}_4^{2-}$  concentration in the vertical distribution were located at 45.19 cm and 2 d, 36.07 cm at 14 d, and 29.85 cm at 26 d following the leaching episode, respectively. At the initial stage after leaching, the peak of  $\text{SO}_4^{2-}$  concentration rapidly moved up. In the medium period, migration was controlled by capillary pressure and penetrated pressure, the multiple ionic charge of  $\text{SO}_4^{2-}$  and the evaporation of liquors; when the capillary pressure and penetrated pressure became weak, the migrated direction of  $\text{SO}_4^{2-}$  changed. The peak of  $\text{SO}_4^{2-}$  moved up to a depth of 36.07 cm after 14 d. Subsequently, the effect of evaporation became stronger, which further resulted in the continuing migration of  $\text{SO}_4^{2-}$ . In the final period, the peak of  $\text{SO}_4^{2-}$  concentration migrated up the upside of the leaching column instead of the bottom.

### 3.5 Potential implication for revegetation

Previously, the management practice of BRDAs has concentrated on containment, with less attention to the changes in long-term leaching of the salinities of the residues in BRDAs. Currently, management projects are moving gradually towards amendment and revegetation to ameliorate the salinity and alkalinity of the stored bauxite residue and/or further soil-formation of BRDAs to reduce environmental hazards associated with natural disposal. Subsequently, this will naturally establish a relatively stable ecosystem in the residue disposal areas, finally reverting to occupied land areas to an alternative option. In this work, a self-designed column was used to simulate the saline migration and distribution of BR in BRDAs during water leaching. The migration characteristics of  $\text{Na}^+$ ,  $\text{CO}_3^{2-}$  and  $\text{HCO}_3^-$  could hinder the efflorescence occurrence of BRDAs' surface, and are helpful to control the salinity by water leaching. Leaching process provides a potential means of ameliorating the high saline and sodic conditions on the surface of BRDAs.

Currently, global inventory of about 4 billion tons of bauxite residue has been stored in BRDAs [30], long-term leaching requires large quantities of water in order to guarantee a steady supply, which may not be

practical in consideration of cost implications. Additionally, it is actual that water should be transported over long distances whilst generating enormously secondary leachate in leaching, which would highlight the potential dam-failure. If the supply of water (perhaps taking full advantage of rainfall) and recovery of leachates (returned to alumina extraction process) could be resolved economically, then water leaching of bauxite residue in BRDAs may be a potential option.

Nevertheless, the surface revegetation of freshly disposed bauxite residue in BRDAs following long-term water leaching has many challenges due to its high salinity and sodic conditions. Recent researches in saline-sodic soils [3,18] have implied that the use of salt resistant halophytes (*Cynodon dactylon* together with *Arbuscular mycorrhizal* fungi and *Arundo donax* L.) would be a potential method to further ameliorate the high saline and sodic conditions and improve the physical and chemical properties on BRDAs' surface. Implication for the revegetation of bauxite residue following long-term leaching that integrates with phytoremediation may be considered as a feasible option.

## 4 Conclusions

1) Water leaching significantly reduced salinity, and leached both saline cations  $\text{Na}^+$ ,  $\text{K}^+$ ,  $\text{Ca}^{2+}$ , and saline anions  $\text{CO}_3^{2-}$ ,  $\text{HCO}_3^-$ ,  $\text{SO}_4^{2-}$  into leachate.

2) The migration capacity of saline cations was in the following decreasing order:  $\text{Na}^+ > \text{K}^+ > \text{Ca}^{2+}$ .  $\text{Na}^+$  and  $\text{K}^+$  initially concentrated at 40–50 cm of the column, and gradually migrated to 20–30 cm at the final stage, whilst  $\text{Ca}^{2+}$  accumulated at depths of 30–40 cm.

3) The migration capacity of saline anions was in the following decreasing order:  $\text{HCO}_3^- > \text{SO}_4^{2-} > \text{CO}_3^{2-}$ , with low migration rate of  $\text{CO}_3^{2-}$  concentrated at 20–30 cm of the column.  $\text{SO}_4^{2-}$  accumulated at depths of 20–30 cm, and  $\text{HCO}_3^-$  migrated to the bottom.

4) The migration characteristics of  $\text{Na}^+$ ,  $\text{CO}_3^{2-}$  and  $\text{HCO}_3^-$  could impede the efflorescence occurrence of BRDAs' surface and are helpful to reduce bauxite residue salinity.

## References

- [1] KONG Xiang-feng, TIAN Tao, XUE Sheng-guo, HARTLEY W, HUANG Long-bin, WU Chuan, LI Chu-xuan. Development of alkaline electrochemical characteristics demonstrates soil formation in bauxite residue undergoing natural rehabilitation [J]. Land Degradation and Development, 2018, 29: 58–67
- [2] XUE Sheng-guo, KONG Xiang-feng, ZHU Feng, HARTLEY W, LI Xiao-fei, LI Yi-wei. Proposal for management and alkalinity transformation of bauxite residue in China [J]. Environmental Science and Pollution Research, 2016, 23: 12822–12834.
- [3] XUE Sheng-guo, ZHU Feng, KONG Xiang-feng, WU Chuan, HUANG Ling, HUANG Nan, HARTLEY W. A review of the characterization and revegetation of bauxite residues (red mud) [J]. Environmental Science and Pollution Research, 2016, 23: 1120–1132.
- [4] ZHU Feng, XUE Sheng-guo, HARTLEY W, HUANG Ling, WU Chuan, LI Xiao-fei. Novel predictors of soil genesis following natural weathering processes of bauxite residues [J]. Environmental Science and Pollution Research, 2016, 23: 2856–2863.
- [5] WU Chuan, HUANG Liu, XUE Sheng-guo, PAN Wei-song, ZOU Qi, HARTLEY W, WONG Ming-hung. Oxidic and anoxic conditions affect arsenic (As) accumulation and arsenite transporter expression in rice [J]. Chemosphere, 2017, 168: 969–975.
- [6] XUE Sheng-guo, SHI Li-zheng, WU Chuan, WU Hui, QIN Yan-yan, PAN Wei-song, HARTLEY W, CUI Meng-qian. Cadmium, lead, and arsenic contamination in paddy soils of a mining area and their exposure effects on human HEPG2 and keratinocyte cell-lines [J]. Environmental Research, 2017, 156: 23–30.
- [7] SAMAL S, RAY A K, BANDOPADHYAY A. Characterization and microstructure observation of sintered red mud-fly ash mixtures at various elevated temperatures [J]. Journal of Cleaner Production, 2015, 101: 368–376.
- [8] KONG Xiang-feng, GUO Ying, XUE Sheng-guo, HARTLEY W, YE Yu-zhen, CHENG Qing-yu. Natural evolution of alkaline characteristics in bauxite residue [J]. Journal of Cleaner Production, 2017, 143: 224–230.
- [9] LIU Wan-chao, CHEN Xiang-qing, LI Wang-xing, YU Yan-fen, YAN Kun. Environmental assessment, management and utilization of red mud in China [J]. Journal of Cleaner Production, 2014, 84: 606–610.
- [10] ZHU Feng, HOU Jing-tao, XUE Sheng-guo, WU Chuan, WANG Qiong-li, HARTLEY W. Vermicompost and gypsum amendments improve aggregate formation in bauxite residue [J]. Land Degradation and Development, 2017, 28: 2109–2120.
- [11] DAVRIS P, BALOMENOS E, PANIAS D, PASPALIARIS I. Selective leaching of rare earth elements from bauxite residue (red mud), using a functionalized hydrophobic ionic liquid [J]. Hydrometallurgy, 2016, 164: 125–135.
- [12] ZHU Feng, LIAO Jia-xin, XUE Sheng-guo, HARTLEY W, ZOU Qi, WU Chuan. Evaluation of aggregate microstructures following natural regeneration in bauxite residue as characterized by synchrotron-based X-ray micro-computed tomography [J]. Science of the Total Environment, 2016, 573: 155–163.
- [13] ZHOU Qiu-sheng, LI Chuang, LI Xiao-bin, PENG Zhi-hong, LIU Gui-hua, QI Tian-gui. Reaction behavior of ferric oxide in system  $\text{Fe}_2\text{O}_3\text{-SiO}_2\text{-Al}_2\text{O}_3$  during reductive sintering process [J]. Transactions of Nonferrous Metals Society of China, 2016, 26: 842–848.
- [14] ZHU Feng, LI Xiao-fei, XUE Sheng-guo, HARTLEY W, WU Chuan, HAN Fu-song. Natural plant colonization improves the physical condition of bauxite residue over time [J]. Environmental Science and Pollution Research, 2016, 23: 22897–22905.
- [15] GRAFE M, POWER G, KLAUBER C. Bauxite residue issues: III. Alkalinity and associated chemistry [J]. Hydrometallurgy, 2011, 108: 60–79.
- [16] ZHU Feng, ZHOU Jia-yi, XUE Sheng-guo, HARTLEY W, WU Chuan, GUO Ying. Aging of bauxite residue in association of regeneration: A comparison of methods to determine aggregate stability & erosion resistance [J]. Ecological Engineering, 2016, 92: 47–54.
- [17] ZHU Feng, HUANG Nan, XUE Sheng-guo, HARTLEY W, HAN Fu-song, LI Yi-wei. Effects of binding materials on micro-aggregate size distribution in bauxite residues [J]. Environmental Science and Pollution Research, 2016, 23: 23867–23875.
- [18] ALSHAAL T, DOMOKOS-SZABOLCSY É, MÁRTON L, CZAKÓ M, KÁTAI J, BALOGH P. Phytoremediation of bauxite-derived red

- mud by giant reed [J]. Environmental Chemistry Letters, 2013, 11: 295–302.
- [19] ZHU Feng, CHENG Qing-yu, XUE Sheng-guo, LI Chu-xuan, WU Chuan, TIAN Tao. Influence of natural regeneration on fractal features of residue microaggregates in bauxite residue disposal areas [J]. Land Degradation and Development, 2018, 29: 138–149.
- [20] ZHU Feng, LI Yu-bing, XUE Sheng-guo, HARTLEY W, WU Hao. Effects of iron–aluminium oxides and organic carbon on aggregate stability of bauxite residues [J]. Environmental Science and Pollution Research, 2016, 23: 9073–9081.
- [21] MENZIES N W, FULTON I M, MORRELL W J. Seawater neutralization of alkaline bauxite residue and implications for revegetation [J]. Journal of Environmental Quality, 2004, 33: 1877–1884.
- [22] KIRWAN L J, HARTSHORN A, MCMONAGLE J B, FLEMING L, FUNNELL D. Chemistry of bauxite residue neutralisation and aspects to implementation [J]. International Journal of Mineral Processing, 2013, 119: 40–50.
- [23] LI Xiao-bin, NIU Fei, TAN Jie, LIU Gui-hua, QI Tian-gui, PENG Zhi-hong, ZHOU Qiu-sheng. Removal of  $S^{2-}$  ion from sodium aluminate solutions with sodium ferrite [J]. Transactions of Nonferrous Metals Society of China, 2016, 26: 1419–1424.
- [24] CLARK M W, JOHNSTON M, REICHEL-TBRUSHETT A J. Comparison of several different neutralisations to a bauxite refinery residue: Potential effectiveness environmental ameliorants [J]. Applied Geochemistry, 2015, 56: 1–10.
- [25] CAPPAL G, DE G G, MUNTONI A, SPIGA D, ZIJLSTRA J J. Combined use of a transformed red mud reactive barrier and electrokinetics for remediation of Cr/As contaminated soil [J]. Chemosphere, 2012, 86: 400–408.
- [26] COURTNEY R, HARRINGTON T. Growth and nutrition of *Holcus lanatus* in bauxite residue amended with combinations of spent mushroom compost and gypsum [J]. Land Degradation and Development, 2012, 23: 144–149.
- [27] COUPERTHWAITTE S J, JOHNSTONE D W, MILLAR G J, FROST R L. Neutralization of acid sulfate solutions using bauxite refinery residues and its derivatives [J]. Industrial & Engineering Chemistry Research, 2013, 52: 1388–1395.
- [28] LIANG Wen-tao, COUPERTHWAITTE S J, KAUR G, YAN Cheng, JOHNSTONE D W, MILLAR G J. Effect of strong acids on red mud structural and fluoride adsorption properties [J]. Journal of Colloid and Interface Science, 2014, 423: 158–165.
- [29] ZHANG Ran, ZHENG Shi-li, MA Shu-hua, ZHANG Yi. Recovery of alumina and alkali in Bayer red mud by the formation of andradite-grossular hydrogarnet in hydrothermal process [J]. Journal of Hazardous Materials, 2011, 189: 827–835.
- [30] KONG Xiang-feng, LI Meng, XUE Sheng-guo, HARTLEY W, CHEN Cheng-rong, WU Chuan, LI Xiao-fei, LI Yi-wei. Acid transformation of bauxite residue: conversion of its alkaline characteristics [J]. Journal of Hazardous Materials, 2017, 324: 382–390.

## 淋溶条件下赤泥盐分离子的迁移与分布

孔祥峰<sup>1,2</sup>, 江星星<sup>1,2</sup>, 薛生国<sup>1,2</sup>, 黄玲<sup>1,2</sup>, William HARTLEY<sup>3</sup>, 吴川<sup>1,2</sup>, 李晓飞<sup>1,2</sup>

1. 中南大学 冶金与环境学院, 长沙 410083;
2. 中南大学 国家重金属污染防治工程技术研究中心, 长沙 410083;
3. Crop and Environment Sciences Department, Harper Adams University, Newport, Shropshire, TF10 8NB, United Kingdom

**摘要:** 赤泥是氧化铝工业生产过程产生的强碱性固体废物, 其盐分含量高, 对环境有害且制约着赤泥堆场的植被重建。通过土柱模拟淋溶实验, 研究赤泥盐离子的动态迁移及垂直分布情况。结果表明: 淋溶不同程度地将赤泥中的  $Na^+$ 、 $K^+$ 、 $Ca^{2+}$ 、 $CO_3^{2-}$ 、 $SO_4^{2-}$  和  $HCO_3^-$  等盐分离子浸出到渗滤液中, 显著降低了赤泥的盐度。赤泥中  $Na^+$  和  $K^+$  呈现出较高的迁移能力, 从柱体的 40~50 cm 处向上迁移至 20~30 cm 处; 而  $Ca^{2+}$  的迁移能力较弱, 主要分布在柱体的 30~40 cm 处。淋溶刚结束时,  $CO_3^{2-}$  主要分布在柱体的 20~30 cm 处, 随后向下迁移至 30~40 cm 处, 最终受蒸发作用迁移至 20~30 cm 处。  $SO_4^{2-}$  最初主要分布在柱体的 40~50 cm 处, 最终向上迁移至 20~30 cm 处。  $HCO_3^-$  主要停留在柱体的下部, 其迁移特性受蒸发的影响较小。

**关键词:** 赤泥; 盐分; 离子迁移; 土柱模拟; 淋溶

(Edited by Wei-ping CHEN)